Ba(OH)$_2$ *Equilibria in the System* Ba-O-H-F, *With Application to the Formation of* Ba$_2$YCu$_3$O$_{6.5+x}$ *From* BaF$_2$-*Precursors*

L. P. Cook and W. Wong-Ng

National Institute of Standards and Technology,
Gaithersburg, MD   20899-8520

and

R. Feenstra

Condensed Matter Sciences Division,
Oak Ridge National Laboratory,
Oak Ridge, TN   37831

lawrence.cook@nist.gov

winnie.wong-ng@nist.gov

f59@ornl.gov

The *ex situ* process for fabricating Ba$_2$YCu$_3$O$_{6.5+x}$ superconducting tapes from BaF$_2$- based precursors involves a hydration/oxidation reaction at ≈730 °C to 750 °C generally written as:

(2 BaF2 + Y + 3 Cu)(amorphous) +
(2 H$_2$O + 2.25 O$_2$)(g) →
Ba$_2$YCu$_3$O$_{6.5+x}$(s) + 4 HF(g).
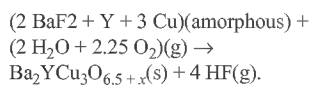
However, microscopic observations of partially processed films suggest the presence of a transient liquid phase during conversion. Alternatively, the conversion reaction can be rewritten as the sum of several intermediate steps, including the formation of a barium hydroxide liquid:

(BaF$_2$)(amorphous) + 2 H$_2$O(g) →
Ba(OH)$_2$(liq) + 2 HF(g).
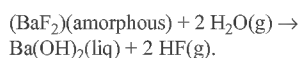
To evaluate the possibility of a hydroxide liquid conversion step, thermodynamic calculations on the stability of Ba(OH)$_2$(liq) have been completed from 500 °C to 900 °C at 0.1 MPa p_{total}. Based on currently available data, the calculated phase diagrams suggest that a viable hydroxide reaction path exists in the higher part of this temperature range. The calculations indicate that Ba(OH)$_2$(liq) may be stable at log p_{H_2O} (Pa) values from ≈4 to 5, provided log p_{HF} (Pa) values can

be maintained below 0 to –1. Limited experimental confirmation is provided by results of an experiment on BaF$_2$(s) at 815 °C, 0.1 MPa p_{H_2O}, in which essentially all F at the surface was replaced by O. It is therefore possible that processing routes exist for producing Ba$_2$YCu$_3$O$_{6.5+x}$ based on the presence of a Ba(OH)$_2$ liquid, which might have an effect on conversion rates and texturing in the superconducting film.
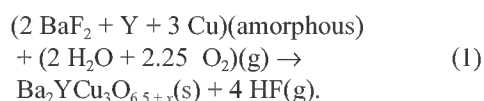
1. Introduction

The development of superconducting Ba$_2$YCu$_3$O$_{6.5+x}$-based tape is continuing at an accelerated pace, with the promise of substantial cost-reductions and performance enhancements in a variety of high temperature super-conductor (high T_c) applications, such as transformer-,

magnet-, and motor-windings and power transmission cables. This technology, the "second generation" of high T_c materials, depends upon the fabrication of superconducting layers deposited on flexible metallic substrates [1-4]. Generally the metallic substrates require deposition of intermediate buffer layers to serve as diffusion barriers at the metal interface, while

promoting textured growth of the overlying oxide superconductor phase. One of the leading processes for producing highly textured second generation "coated conductors" is the "BaF$_2$ *ex situ*" method [5-7], a process which consists of two principal steps. In the first step, amorphous films having (2 BaF$_2$ + Y + 3 Cu) stoichiometry are deposited on the buffer layer by physical vapor deposition (PVD) or metal/organic deposition (MOD) techniques. The second step (shown diagrammatically in Fig. 1) involves the conversion of the amorphous film to superconducting material, nominally according to the following overall reaction:

$$(2 \text{ BaF}_2 + \text{Y} + 3 \text{ Cu})(\text{amorphous})$$
$$+ (2 \text{ H}_2\text{O} + 2.25 \text{ O}_2)(\text{g}) \rightarrow \qquad (1)$$
$$\text{Ba}_2\text{YCu}_3\text{O}_{6.5+x}(\text{s}) + 4 \text{ HF(g)}.$$

Typically, the reaction takes place at ≈730 °C to 750 °C. The principal advantages of the *ex situ* process are that the first step is a relatively simple, rapid operation completed without the necessity of substrate heating, and that the second, more time-consuming step can be completed separately from the deposition process, without the need for vacuum conditions. The exact nature of the conversion process remains controversial. Indirect evidence has been presented for the formation of an amorphous intermediate phase (possibly a liquid) during the conversion [8].

2. Previous Work

Research has previously been conducted in our laboratory to determine the nature of low-melting-temperature liquids involved in the BaF$_2$ *ex situ* conversion [9-11]. The relevant phase equilibria can be discussed with reference to the Ba,Y,Cu//O,F quaternary reciprocal system, portrayed in Fig. 2a as a trigonal prism in compositional phase space. Initially, the relative thermodynamic stabilities of Table 1 were used to subdivide the trigonal prism of Fig. 2a into its constituent tetrahedra, shown in Fig. 2b. The phase stabilities defining these tetrahedra have since been confirmed experimentally, and hence the tetrahedra serve as a valid outline for discussion of the conversion process. In traversing along a compositional vector from the oxides at the base of the trigonal prism, to the fluorides at the top, the three constituent tetrahedra encountered are: BaF$_2$-BaO-½Y$_2$O$_3$-CuO$_x$, BaF$_2$-YF$_3$-½Y$_2$O$_3$-CuO$_x$, and BaF$_2$-YF$_3$-CuF$_2$-CuO$_x$. The first two tetrahedra share the very stable BaF$_2$-½Y$_2$O$_3$-CuO$_x$ compositional plane, where the ideal compositions of PVD precursor films would be plotted. In terms of fluoride/oxide ratio, the progression of such films during *ex situ* conversion to superconductor would ideally follow the path shown in the lower tetrahedron of Fig. 2b. Yet, melting temperatures below 815 °C were not found in this tetrahedron, even in the presence of
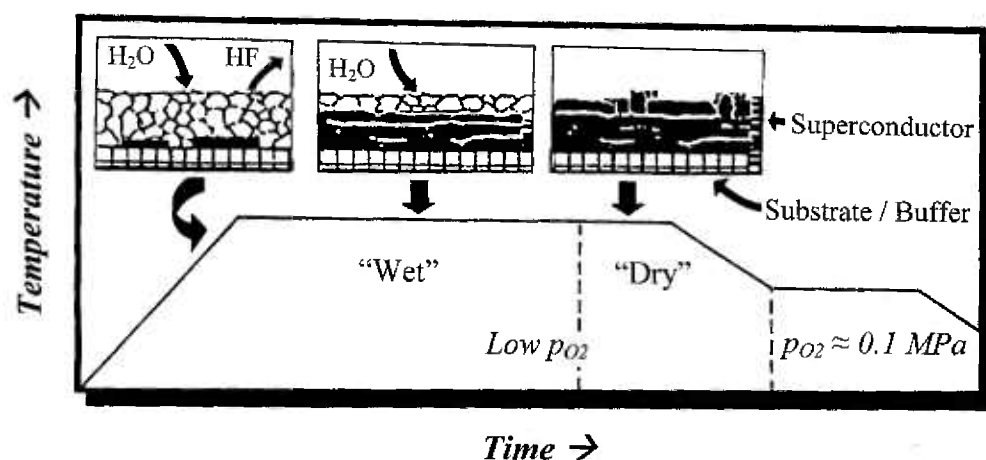

Fig. 1. Schematic illustration of the "BaF$_2$ *ex situ*" process for fabrication of Ba$_2$YCu$_3$O$_{6.5+x}$ coated conductors, showing conversion of precursor film (top), as deposited on substrate/buffer layer. Precursor is converted starting at buffer/precursor interface by reaction with water vapor entering from top. Superconductor layer (dark) grows and is then annealed at lower temperatures under dry conditions in oxygen.
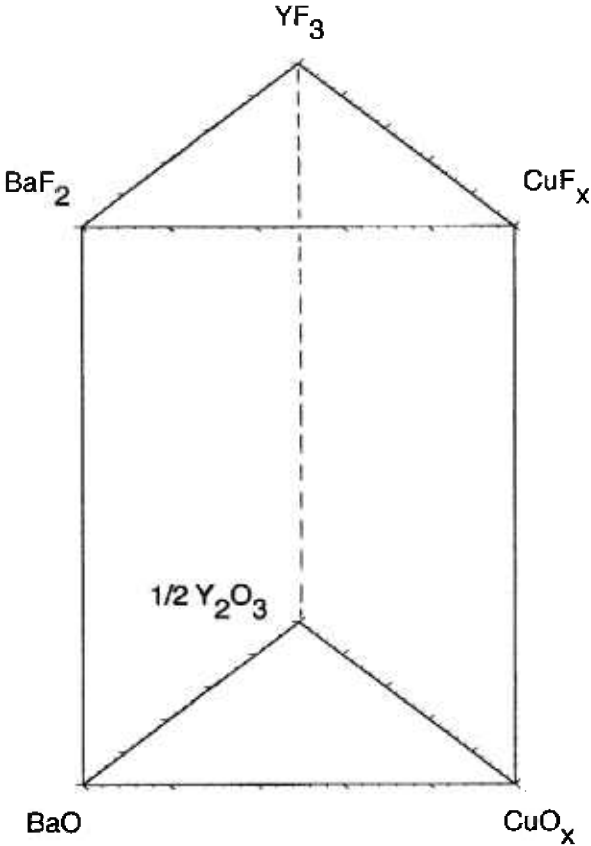
Fig. 2a. Trigonal prism used for compositional model of BaF_2 *ex situ* phase equilibria.

Table 1. Relative thermodynamic stabilities in the system Ba, Y, Cu//O. F at 500 °C, 0.1 MPa (reactants and products in most stable form)

Reactants		Products	Gibbs energy of reaction
$3 CuF_2 + Y_2O_3$	$\rightarrow$	$3 CuO + 2 YF_3$	-396 kJ
$2 YF_3 + 3 BaO$	$\rightarrow$	$3 BaF_2 + Y_2O_3$	-413 kJ
$CuF_2 + BaO$	$\rightarrow$	$BaF_2 + CuO$	-270 kJ

H_2O-containing gas mixtures with reduced p_{O_2}. Locally, it is possible that PVD compositions might deviate from the BaF_2-$\frac{1}{2}Y_2O_3$-CuO plane in the fluoride-direction. Also, MOD films initially have compositions with more fluoride than would correspond to compositions in this plane. Therefore our search for low-melting liquids was also extended into the fluoride-rich regions of Fig. 2. Our experimental investigation of the BaF_2-YF_3-$\frac{1}{2}Y_2O_3$-CuO_x tetrahedron has shown that melting temperatures in that tetrahedron are in excess of 800 °C, even in the presence of H_2O, or with reduced p_{O_2}.

In the BaF_2-YF_3-CuF_2-CuO_x tetrahedron, fluoride-rich liquids melting as low as 580 °C were found; possibly these could be involved in the early stages of MOD
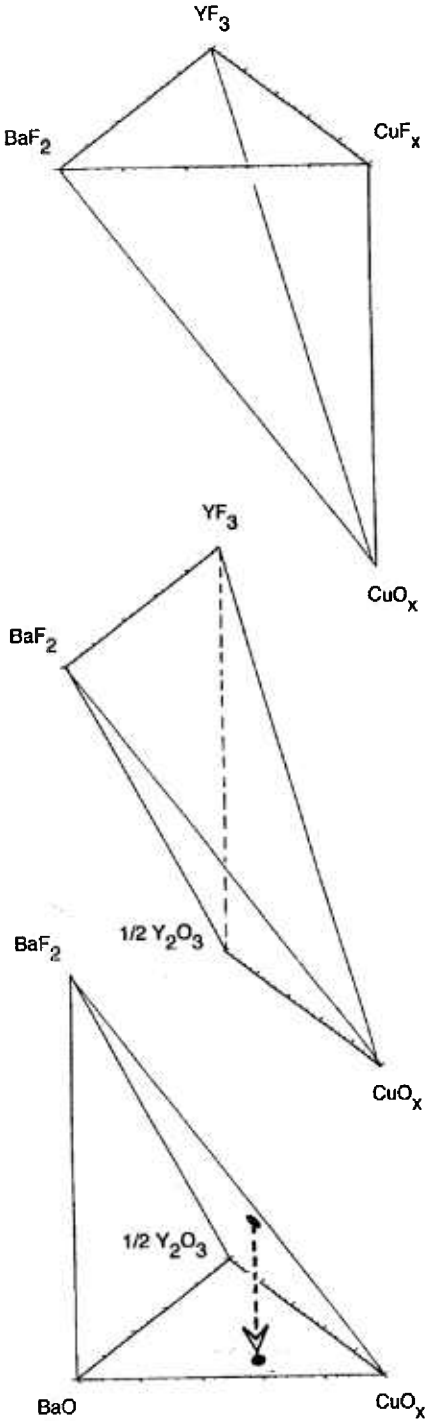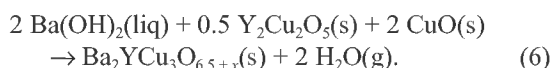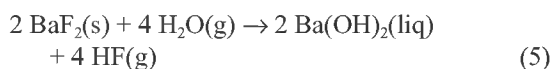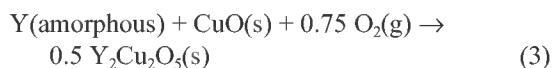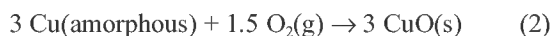

Fig. 2b. Phase compatibility tetrahedra comprising the trigonal prism. Idealized *ex situ* processing path for PVD films is shown in bottom tetrahedron.

film conversion. However, for low-melting liquids to be generally operative in conversion of both PVD and MOD films, they would need to lie closer in phase space to the BaF_2-½Y_2O_3-CuO_x plane. Consequently, our search for low-melting liquids has turned to the possible presence of $Ba(OH)_2$, a compound known to melt much lower (at ≈ 408 °C) [12] than the other phases and components of the Ba,Y,Cu//O,F system. Under suitable p_{H_2O} and temperature, $Ba(OH)_2$ could proxy for the BaO component.

3. Possible Presence of $Ba(OH)_2$ During *Ex Situ* Conversion

Reaction (1) may be rewritten as the sum of several constituent reactions, based in part on high temperature powder x-ray diffraction (HTXRD) observations in our laboratory [10,13] and in other laboratories [14,15]. Moreover, under sufficiently high p_{H_2O}, the BaO component of Fig. 2 could effectively be replaced by $Ba(OH)_2$, resulting in the following conversion steps:

$$3 \text{ Cu(amorphous)} + 1.5 \text{ O}_2(g) \rightarrow 3 \text{ CuO(s)} \qquad (2)$$

$$\begin{aligned} &\text{Y(amorphous)} + \text{CuO(s)} + 0.75 \text{ O}_2(g) \rightarrow \\ &\quad 0.5 \text{ Y}_2\text{Cu}_2\text{O}_5(s) \end{aligned} \qquad (3)$$

$$2 \text{ BaF}_2(\text{amorphous}) \rightarrow 2 \text{ BaF}_2(s) \qquad (4)$$

$$\begin{aligned} &2 \text{ BaF}_2(s) + 4 \text{ H}_2\text{O}(g) \rightarrow 2 \text{ Ba(OH)}_2(\text{liq}) \\ &\quad + 4 \text{ HF}(g) \end{aligned} \qquad (5)$$

$$\begin{aligned} &2 \text{ Ba(OH)}_2(\text{liq}) + 0.5 \text{ Y}_2\text{Cu}_2\text{O}_5(s) + 2 \text{ CuO(s)} \\ &\quad \rightarrow \text{Ba}_2\text{YCu}_3\text{O}_{6.5+x}(s) + 2 \text{ H}_2\text{O}(g). \end{aligned} \qquad (6)$$

Reactions (5) and (6) indicate the presence of $Ba(OH)_2$ liquid as an intermediate step.

4. Goal and Approach of Present Investigation

The primary goal of this paper is to evaluate the possible presence of $Ba(OH)_2$ liquid during the *ex situ* conversion process, using a combination of experimental and calculative methods. Demonstrating the presence of liquids at high temperature is of course is not possible by HTXRD, and so we must rely on less direct methods. Also, maintaining the high p_{H_2O} and low p_{HF} thought necessary to form $Ba(OH)_2$ liquids from BaF_2 at high temperature in a controlled experimental environment is in itself a daunting task. For this purpose, we constructed a special high-flow steam furnace, as

described below. We have completed extensive equilibrium calculations on the stability of $Ba(OH)_2$ liquids using available thermodynamic data, including the effect of CO_2 contamination. Based on the calculated stabilities, we designed experiments using the high-flow steam furnace to test for the formation $Ba(OH)_2$(liq) according to its predicted stability field. As a background for this work, differential thermal analysis (DTA) experiments were completed on carefully chosen compositions.

5. Experimental Procedure[1]

BaO was synthesized from 99.99 % purity (metals, by mass) $BaCO_3$ by vacuum-calcining at 1300 °C for 10 h, followed by transfer to a glovebox. Complete decarbonation and conversion to BaO were verified by x-ray powder diffraction (XRD) in a sealed x-ray mount [16]. Powder XRD was completed on a Philips 2θ diffractometer[1] using Cu K_α radiation and a graphite monochromator. Diffractometer control and data acquisition were achieved using the JADE software system.

For melting studies, a $Ba(OH)_2$/BaO mixture was prepared by controlled hydration of BaO. Melting and annealing experiments with simultaneous differential thermal analysis/thermogravimetric analysis (DTA/TGA) were completed in a Mettler TA1 thermoanalyzer outfitted with Anatech digital control and data acquisition electronics. DTA was completed at a ramp rate of 10 °C/min. The DTA apparatus was calibrated against the α/β quartz transition (571 °C) and the NaCl melting point (801 °C); DTA temperatures are estimated to have < ± 3 °C standard uncertainty. DTA crucibles were of dense slip-cast MgO.

To enable experiments at high p_{H_2O}, a furnace capable of operation up to $p_{H_2O} = (0.1 \text{ MPa})$ at temperatures above 800 °C was constructed, as shown schematically in Fig. 3. The special features of this furnace are: 1. a 3 kW steam generator provides an approximately constant-pressure source of steam for the furnace; 2. the steam generator uses a water feedstock with reduced CO_2 (discussed below); 3. all areas of the furnace and supply lines are maintained at >100 °C; 4. a type S thermocouple is positioned in the base of

---

[1] Certain commercial equipment, instruments, or materials are identified in this paper to foster understanding. Such identification does not imply recommendation or endorsement by the National Institute of Standards and Technology, nor does it imply that the materials or equipment identified are necessarily the best available for the purpose.
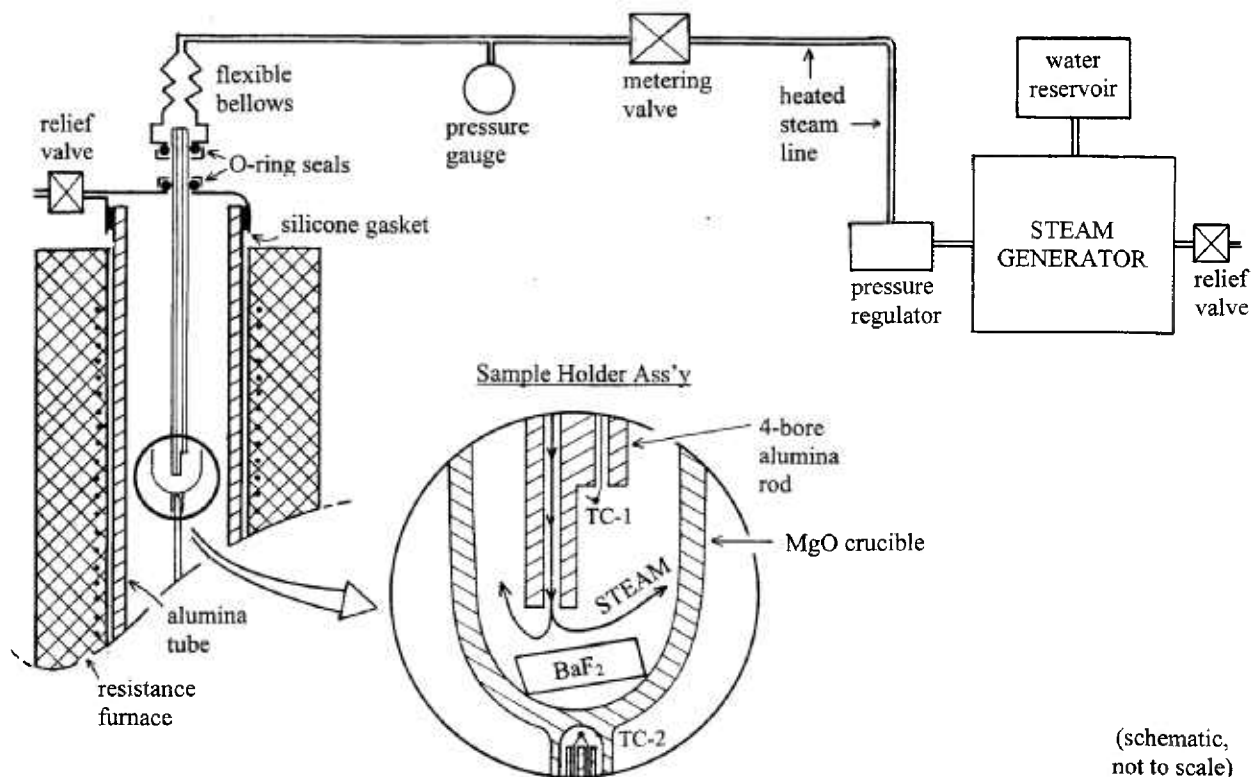
Fig. 3. Schematic diagram of steam furnace set-up for generation of high p_{H_2O} with rapid flow rates at elevated temperatures.

the sample crucible within 2 mm of the sample (TC-2); 5. the steam inlet is positioned in the crucible directly above the sample such that the steam flow must circulate around the sample before exiting the crucible; 6. steam flow can be reproducibly metered via a heated control valve; 7. a rapid flow of steam directly over the sample is possible. Steam furnace experimental results were examined optically using a Leica Wild M10 stereomicroscope and SPOT digital image capture software. Results were also characterized with an AMRAY 1400 scanning electron microscope (SEM) operated at ≈ 20 kV. Elemental compositions were determined with a Gresham energy dispersive x-ray spectrometer (EDS) and a 4Pi Analysis data acquisition interface controlled by Revolution software.

6. Calculative Procedure

Solid-liquid-gas equilibria in the system $Ba(OH)_2$-BaO-BaF_2-H_2O-HF (and also with CO_2) were calculated as a function of temperature using the Janaf thermochemical database [17] and the FactSage software suite [18]. The latter uses a Gibbs energy minimization algorithm to calculate equilibrium concentrations of

species in the gas phase, and to calculate activities of liquid and solid phases. The calculative procedure involves minimizing the total stoichiometric summation of terms:

$$G(i,T) = \left(\Delta_f H^{\circ}_m (i, 298) + \int_{298}^{T} C_p(i)\, d\,T \right)$$

$$-T \left(S^{\circ}(i, 298) + \int_{298}^{T} C_p(i)/T d\,T \right) \tag{7}$$

for the collection of phases being considered, where $G(i,T)$ = Gibbs energy function for phase i, $\Delta_f H^{\circ}_m(i, 298)$ = standard molar enthalpy of formation for phase i, $S^{\circ}(i, 298)$ = absolute molar entropy for phase i, $C_p(i)$ = molar heat capacity of phase i at constant pressure (0.1 MPa) , and T = temperature kelvin. For solution phases, appropriate mixing terms must be added to Eq. (7), including terms of the form $RT\ln(p_j)$, where R = gas constant and p_j = activity or partial pressure of species j. Species considered in the calculations are shown in Table 2. For the present calculations, gaseous species were considered to mix ideally. As described

below, for purposes of calculation we assume there is negligible solubility of BaO and BaF_2 in $Ba(OH)_2$ liquids at the eutectic. Therefore to a first approximation the liquids are simple liquids, essentially pure. With regard to solid phases, there is evidence for solid solution of BaO in BaF_2 [19], although a quantitative determination has not been made, and the extent is not known. Also, existence of a compound intermediate between BaF_2 and $Ba(OH)_2$ has been proposed [15]. As yet, there has been no definitive proof of such a compound, and there is no published x-ray diffraction pattern in the Powder Diffraction File [20]. However, it is clear that refinements in the calculations will need to be made, if additional data become available. For the present, the calculations give an approximate idea of the $Ba(OH)_2$(liq) stability field. It is expected that solubility of BaF_2 or BaO in $Ba(OH)_2$(liq) would expand the liquid field of stability, whereas existence of an intermediate compound would have the opposite effect.

Table 2. Gaseous species and condensed phases included in $Ba(OH)_2$/BaO/BaF_2 equilibrium calculations

Gaseous species	Solids	Liquids
$H, H_2, O, O_2, O_3, OH, H_2O, HOO,$	$BaF_2, BaO,$	$Ba, BaO, Ba(OH)_2$
$HOOH, F, F_2, HF, (HF)_2, H_3F_3, H_4F_4,$	$Ba(OH)_2,$	BaF_2
$H_5F_5, H_6F_6, H_7F_7, OF, O_2F, HOF, Ba,$	$Ba(OH)_2 \cdot 8H_2O$	
$Ba_2, BaH, BaH_2, BaO, Ba_2O, Ba_2O_2,$		
$BaOH, Ba(OH)_2, BaF, BaF_2,$		

7. Effect of p_{CO_2} on $Ba(OH)_2$ Equilibria

One of the reasons for the relative success of the BaF_2 *ex situ* method is the elimination of carbonate (usually present as $BaCO_3$) from the processing route. Carbonate not only affects the kinetics of $Ba_2YCu_3O_{6.5+x}$(s) formation due to the relative stability of $BaCO_3$(s), but also affects the equilibrium phase assemblage by favoring formation of oxycarbonate phases such as $Ba_4Y_2O_7 \cdot xCO_2$ and $Ba_2Y_2O_5 \cdot xCO_2$ [21,22]. Formation of these phases interferes with $Ba_2YCu_3O_{6.5+x}$(s) formation and complicates the decarbonation reactions which must take place for formation of $Ba_2YCu_3O_{6.5+x}$(s) from $BaCO_3$-containing precursors. Furthermore, presence of carbon in the superconductor phase has been shown to adversely affect properties [23].

Calculations have been performed to estimate the effect of CO_2 on $Ba(OH)_2$ equilibria, by adding CO_2(g), three polymorphs of $BaCO_3$(s), and $BaCO_3$(liq) to the list of species considered in Table 2. These calculations have been completed to determine the values of p_{H_2O}

and p_{CO_2} which are in equilibrium with coexisting $Ba(OH)_2$ and $BaCO_3$, as shown in Fig. 4. From the curves in Fig. 4, at 500 °C, a p_{CO_2} of $< 10^{-4.6}$ Pa is required to avoid formation of $BaCO_3$, while a p_{H_2O} of $> 10^{1.8}$ Pa) is necessary to stabilize $Ba(OH)_2$. At 900 °C, p_{CO_2} must be $< 10^{1.4}$ Pa) to avoid formation of $BaCO_3$, and p_{H_2O} of $> 10^{4.5}$ Pa is required to stabilize $Ba(OH)_2$. For comparison, at 25 °C, water in equilibrium with air $(p_{CO_2} = 10^{1.5}$ Pa) contains $\approx 10^{-7}$ mol fraction dissolved CO_2. Water of this composition, if vaporized, would be within the $BaCO_3$ stability field up to ≈ 625 °C. At 99 °C, water in equilibrium with air contains $\approx 10^{-9}$ mole fraction CO_2, and if vaporized, would fall below the $BaCO_3$ stability line above ≈ 525 °C. From these calculations it is clear that water used to generate p_{H_2O} must be heated to reduce CO_2 content if formation of $BaCO_3$ is to be avoided. This is especially critical in experiments involving the formation of $Ba(OH)_2$, such as those discussed below.
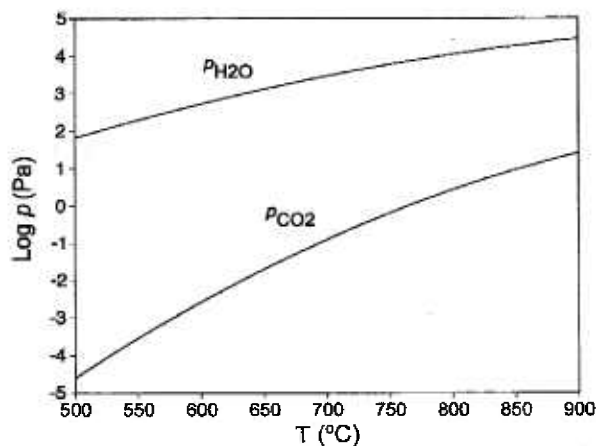

Fig. 4. Equilibrium partial pressures of H_2O and CO_2 over coexisting $Ba(OH)_2$ and $BaCO_3$ as a function of temperature.

8. $Ba(OH)_2$/BaO

The melting of a $Ba(OH)_2$/BaO mixture was investigated by DTA to estimate the effect of BaO solubility on the melting temperature. A lowering of ≈ 3 °C was found, which lies within the estimated uncertainty of the DTA measurements. It is therefore concluded that the solubility of BaO in $Ba(OH)_2$ liquids is negligible, and that $Ba(OH)_2$ liquid can be modeled for calculational purposes as essentially pure $Ba(OH)_2$.

Accordingly, equilibria between solid and liquid $Ba(OH)_2$ and BaO(s) were calculated and are presented in the phase diagram of Fig. 5. At $p_{H_2O} = 0.1$ MPa, $Ba(OH)_2$(liq) is stable up to ≈ 1051 °C. At lower temperatures, the $Ba(OH)_2$(s) stability field extends to
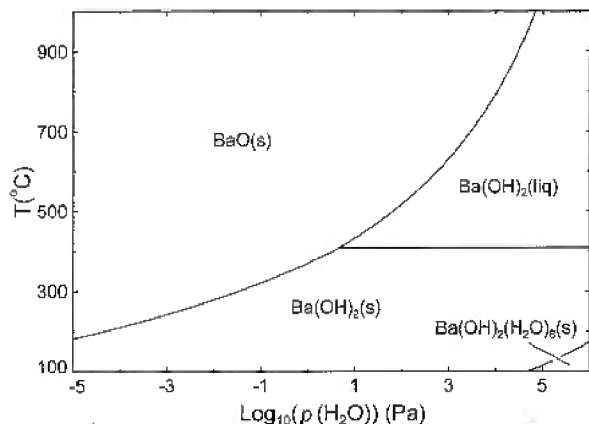
Fig. 5. Log p_{H_2O}-T phase diagram of the system BaO-H$_2$O calculated using available thermodynamic data [17, 18].

Fig. 6. Ba(OH)$_2$/BaO equilibrium as a function of log p_{H_2O} and log p_{HF}.

very low values of p_{H_2O} (< 10^{-10} Pa). The Ba(OH)$_2$(liq) stability field is confined to a relatively narrow slice of the phase diagram above $p_{H_2O} \approx 10$ Pa, lying between the phase fields of BaO(s) and Ba(OH)$_2$(s). The most abundant gaseous species in equilibrium with Ba(OH)$_2$(liq) along the Ba(OH)$_2$(liq)/BaO(s) equilibrium curve are shown for selected temperatures in Table 3. While p_{H_2O} is several orders of magnitude above the other partial pressures, it is noteworthy that at 900 °C, $p_{Ba(OH)_2}$ reaches ≈ 1 Pa. A partial pressure of this magnitude is sufficient to cause significant mass transport of Ba(OH)$_2$ in the gas phase. At 25 °C (not shown in Fig. 5 or Table 3), the calculated p_{H_2O} over coexisting Ba(OH)$_2$(s) and BaO(s) is estimated to be 10^{-14} Pa, an indication of the difficulty in storing and handling BaO.

with increasing temperature. Above this value, indicated by the dashed parts of the equilibrium lines at any given temperature, the Ba(OH)$_2$(liq)/BaO(s) equilibrium is metastable. Gas phase compositions for selected points near the centers of the equilibrium boundaries in Fig. 6 are given in Table 4. Comparison of Table 3 and Table 4 reaffirms the constancy of the equilibrium p_{H_2O} in the presence of HF.

Table 3. Gas phase partial pressures (Pa) in equilibrium with Ba(OH)$_2$(liq)/BaO(s)

T(°C)	p_{H_2O}	p_{H_2}	$p_{Ba(OH)_2}$	p_{O_2}	p_{OH}
500	$10^{1.8}$	$10^{-6.3}$	$10^{-6.4}$	$10^{-6.6}$	$10^{-8.2}$
600	$10^{2.7}$	$10^{-4.4}$	$10^{-4.2}$	$10^{-4.7}$	$10^{-6.0}$
700	$10^{3.5}$	$10^{-2.8}$	$10^{-2.5}$	$10^{-3.2}$	$10^{-4.3}$
800	$10^{4.0}$	$10^{-1.7}$	$10^{-1.2}$	$10^{-2.0}$	$10^{-2.9}$
900	$10^{4.5}$	$10^{-0.7}$	$10^{-0.1}$	$10^{-1.0}$	$10^{-1.8}$

Table 4. Gas phase partial pressures (Pa) in equilibrium with Ba(OH)$_2$(liq)/BaO(s) in the presence of HF

T(°C)	p_{H_2O}	p_{HF}	p_{H_2}	$p_{Ba(OH)_2}$	p_{O_2}	p_{OH}
500	$10^{1.8}$	$10^{-6.3}$	$10^{-6.3}$	$10^{-6.4}$	$10^{-6.6}$	$10^{-8.2}$
600	$10^{2.7}$	$10^{-5.5}$	$10^{-4.4}$	$10^{-4.3}$	$10^{-4.7}$	$10^{-6.0}$
700	$10^{3.5}$	$10^{-5.0}$	$10^{-2.9}$	$10^{-2.5}$	$10^{-3.2}$	$10^{-4.3}$
800	$10^{4.0}$	$10^{-4.3}$	$10^{-1.7}$	$10^{-1.2}$	$10^{-2.0}$	$10^{-2.9}$
900	$10^{4.5}$	$10^{-3.9}$	$10^{-1.7}$	$10^{-0.1}$	$10^{-1.0}$	$10^{-1.3}$

The effect of HF(g) *ex situ* conversion product on Ba(OH)$_2$(liq)/BaO(s) equilibria must also be considered. As shown in Fig. 6, the log p_{H_2O} values for the Ba(OH)$_2$(liq)/BaO(s) equilibrium remain constant and independent of log p_{HF} for any given temperature. However the maximum value of log p_{HF} to which the Ba(OH)$_2$(liq)/BaO(s) equilibrium is stable increases

9. Ba(OH)$_2$/BaF$_2$

Due to the formation of Ba(OH)$_2$-hydrates, it was not possible to prepare pure Ba(OH)$_2$ from BaO during this investigation, and therefore the melting point lowering of Ba(OH)$_2$/BaF$_2$ mixtures was not investigated experimentally. For calculational purposes it is therefore

assumed that the solubility of BaF_2 in $Ba(OH)_2(liq)$ at the eutectic is small, a reasonable assumption, given the much higher melting point of BaF_2 (> 1300 °C).

To describe the equilibrium between $Ba(OH)_2(liq)$ and $BaF_2(s)$, it is necessary to consider p_{HF} as well as p_{H_2O}. Figure 7 shows calculated curves for the $Ba(OH)_2(liq)/ BaF_2(s)$ equilibrium at several temperatures. As the temperature increases, the maximum p_{HF} value to which the $Ba(OH)_2(liq)$ stability field extends increases. As temperature increases, the minimum p_{H_2O} value to which the $Ba(OH)_2(liq)$ stability field extends also increases. Below this value, the $Ba(OH)_2(liq)/BaF_2(s)$ equilibrium is metastable. Gas phase compositions at selected points on the curves in Fig. 7 are given in Table 5. At higher temperatures, as for the $Ba(OH)_2(liq)/BaO(s)$ equilibrium, the values of $p_{Ba(OH)_2}$ become significant. From the slopes of Fig. 7 and the data in Table 5, a given increase in p_{H_2O} results in a proportionately much larger increase in the equilibrium p_{HF}. For example, an order-of-magnitude increase in p_{H_2O} produces a two orders-of-magnitude increase in p_{HF}. The requirements for HF(g) removal during the conversion of $BaF_2(s)$ to $Ba(OH)_2(liq)$ are significantly reduced by maintaining increased p_{H_2O}, as well as by maintaining higher temperatures.

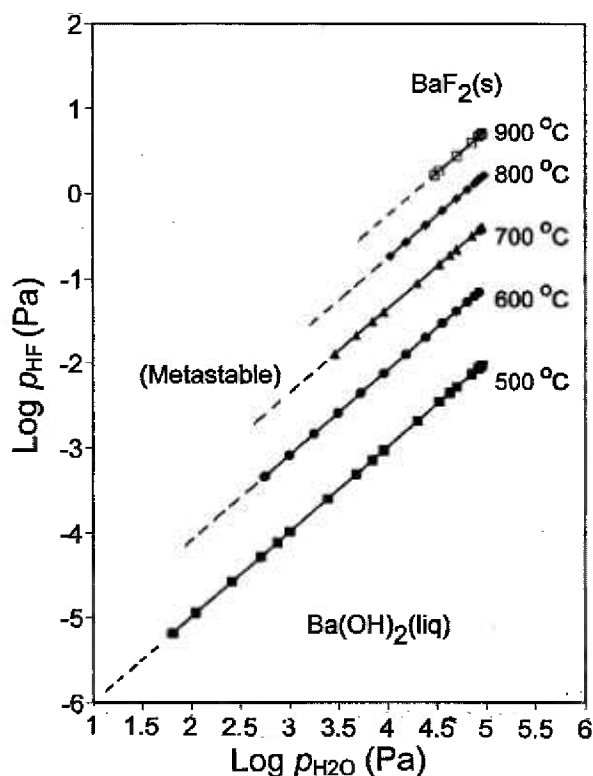**Table 5.** Gas phase partial pressures (Pa) in equilibrium with $Ba(OH)_2(liq)/BaF_2(s)$

$T(°C)$	p_{H_2O}	p_{HF}	p_{H_2}	$p_{Ba(OH)_2}$	p_{O_2}	p_{OH}
500	$10^{3.4}$	$10^{-3.6}$	$10^{-5.2}$	$10^{-6.4}$	$10^{-5.5}$	$10^{-7.2}$
600	$10^{4.0}$	$10^{-2.1}$	$10^{-3.6}$	$10^{-4.2}$	$10^{-3.9}$	$10^{-5.2}$
700	$10^{4.3}$	$10^{-1.1}$	$10^{-2.3}$	$10^{-2.5}$	$10^{-2.6}$	$10^{-3.7}$
800	$10^{4.6}$	$10^{-0.2}$	$10^{-1.3}$	$10^{-1.2}$	$10^{-1.6}$	$10^{-2.6}$
900	$10^{4.7}$	$10^{0.4}$	$10^{-0.6}$	$10^{-0.1}$	$10^{-0.8}$	$10^{-1.6}$

10. $Ba(OH)_2/BaO/BaF_2$

Treatment of equilibria involving the three phases $Ba(OH)_2$, BaO, and BaF_2 is facilitated by the use of the 3-D plot shown in Fig. 8, where the three-phase $Ba(OH)_2/BaO/BaF_2$ equilibrium is represented as a function of p_{H_2O}, p_{HF}, and temperature. The three-phase equilibrium is actually a curve in log p_{H_2O} - log p_{HF} - temperature parameter space, as illustrated by its projection onto the base of the plot. Table 6 gives gas phase compositions at selected points along the three-phase equilibrium.
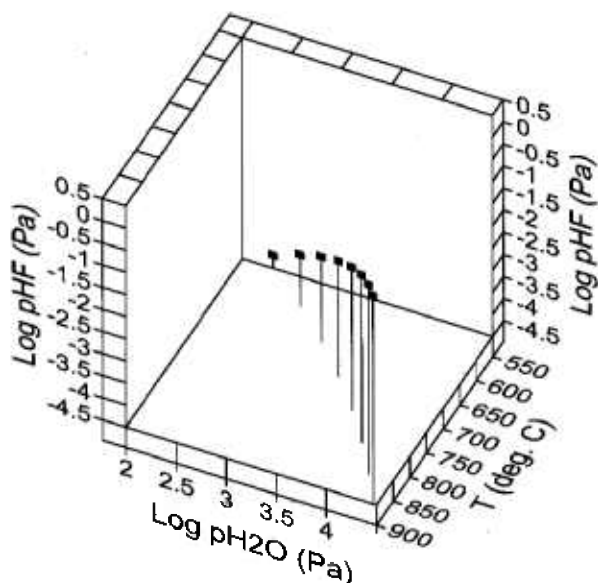

Fig. 8. Three-phase $Ba(OH)_2/BaO/BaF_2$ equilibrium as a function of log p_{H_2O}, log p_{HF}, and temperature. Dashed lines indicate orthogonal projection of the equilibrium curve onto the sidewalls of the 3-D plot.

The data in Fig. 8 can also be conveniently represented through the use of isothermal sections, as shown in Fig. 9. Here the three-phase $Ba(OH)_2/BaO/BaF_2$ equilibrium plots as a point at the juncture of the areas

Fig. 7. $Ba(OH)_2/BaF_2$ equilibrium as a function of log p_{H_2O} and log p_{HF}.

Table 6. Gas phase partial pressures (Pa) in equilibrium with $Ba(OH)_2(liq)/BaO(s)/BaF_2(s)$

$T(°C)$	p_{H_2O}	p_{HF}	p_{H_2}	$p_{Ba(OH)_2}$	p_{O_2}	p_{OH}
500	$10^{1.8}$	$10^{-5.2}$	$10^{-6.3}$	$10^{-6.4}$	$10^{-6.6}$	$10^{-8.2}$
600	$10^{2.7}$	$10^{-3.3}$	$10^{-4.4}$	$10^{-4.2}$	$10^{-4.7}$	$10^{-6.0}$
700	$10^{3.5}$	$10^{-5.0}$	$10^{-2.9}$	$10^{-2.5}$	$10^{-3.2}$	$10^{-4.3}$
800	$10^{4.0}$	$10^{-4.3}$	$10^{-1.7}$	$10^{-1.2}$	$10^{-2.0}$	$10^{-2.9}$
900	$10^{4.5}$	$10^{-3.9}$	$10^{-1.7}$	$10^{-0.1}$	$10^{-1.0}$	$10^{-1.3}$
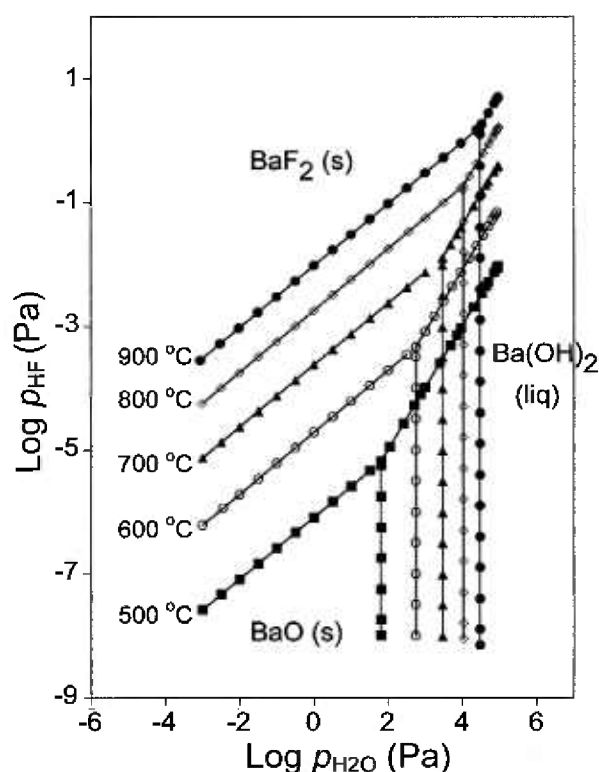
Fig. 9. Isothermal sections through three-phase $Ba(OH)_2/BaO/BaF_2$ region in Fig. 8.

corresponding to the $Ba(OH)_2$, BaO, and BaF_2 stability fields. With increasing temperature, the stability field of $Ba(OH)_2$ shrinks to higher p_{H_2O}, but simultaneously expands to higher p_{HF}.

On the basis of Fig. 9, a steam furnace experiment was designed to test for the formation of $Ba(OH)_2(liq)$ from $BaF_2(s)$. Using the steam furnace, p_{H_2O} of 0.1 MPa at temperatures of 800 °C or above can be maintained for extended periods of time. These are the optimum conditions for formation of $Ba(OH)_2(liq)$ according to reaction (5), provided p_{HF} can be maintained at < 1 Pa. In practice, the latter requirement can be met by rapid-ly flowing steam over the sample to remove product HF, thereby reducing p_{HF} to low levels.

Results of a steam furnace experiment in which a single crystal fragment of optical quality BaF_2 was held at 815 °C, for 2h, with $p_{H_2O} = 0.1$ MPa, with a steam flow over the sample estimated at > 0.2 L/s, are shown in Fig. 10a. Fluorine on the surface of the BaF_2 has been uniformly replaced by oxygen to a depth of at least 1 μm, as estimated by the lack of a fluorine EDS signal from the underlying BaF_2 (Fig. 10b). The full EDS spectrum (not presented) shows Ba and O as the main constituents on the surface of the reacted crystal, with a relatively small C K_α peak (no method was available for detection of hydrogen). The smooth, dense nature of the reacted surface is consistent with the formation of $Ba(OH)_2$ liquid. As discussed above, CO_2 in the water feedstock for this experiment was reduced to low levels such that the formation of $BaCO_3$ was minimized. The EDS spectrum of Fig. 10b indicates that $BaCO_3$ was not a major reaction product, as the C K_α intensity is similarly low for both reacted and unreacted crystals. The presence of C in both spectra is an indication of minor hydrocarbon surface contamination. Smaller peaks present in the reacted sample are due to trace contaminants from the steam boiler and transport line (Si, possibly Co), and are not likely to have had a significant effect on the F/O reaction. We conclude that formation of $Ba(OH)_2(liq)$ from $BaF_2(s)$ according to reaction (5) is the most probable explanation of the results in Fig. 10.

The high-flow experiment at 815 °C, $p_{H_2O} = 0.1$ MPa may be near the upper limit of conditions useful for practical processing of second-generation coated conductors, due to the thermal limitations of currently available substrate/buffer combinations. From Fig. 9, production of $Ba(OH)_2$ liquids at lower temperatures requires more complete removal of HF from the reaction site. An estimate of the requirements for $Ba(OH)_2(liq)$ formation according to reaction (5) at 700 °C can be made as follows. First, it must be noted that, at 700 °C, p_{HF} must be $\approx < 10^{-1}$ Pa for $Ba(OH)_2(liq)$ to form. At a steam flow rate of 0.2 L/s over the sample, this gives a maximum HF removal of $10^{-3.8}$ mL/s from the reaction site, assuming equilibrium. The resulting rate of formation of $Ba(OH)(liq)$ is $10^{-8.1}$ mol/s. If reaction (5) is the rate-limiting step, then $Ba_2YCu_3O_{6.5+x}$ would be formed by reaction (6) at a rate of $\approx 10^{-8.4}$ mol/s. For a 1 cm^2 area, this corresponds to a thickness conversion rate of $\approx 10^{-2.3}$ μm/s at 700 °C. Thus, formation of $Ba_2YCu_3O_{6.5+x}$ superconducting films of 1 μm thickness over an area of 1 cm^2 could conceivably be achieved in 200 s to 250 s, with potential for scale-up
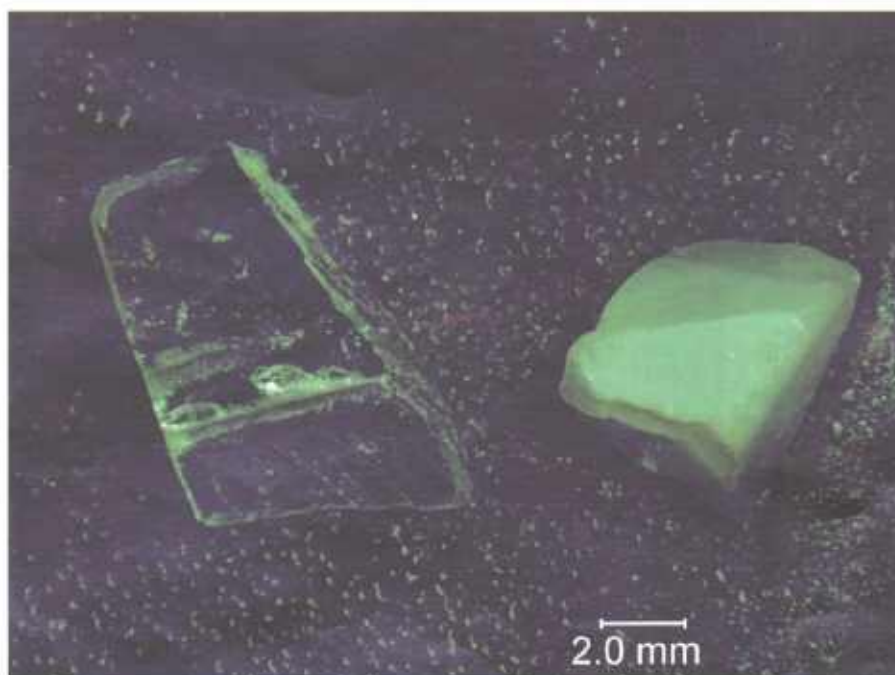
Fig. 10a. Results of BaF_2 single crystal placed in steam furnace at 815 °C, 2 h, p_{H_2O} = 0.1 MPa. Clear crystal on left is unreacted. Reaction produced dense white opaque coating on crystal at right.
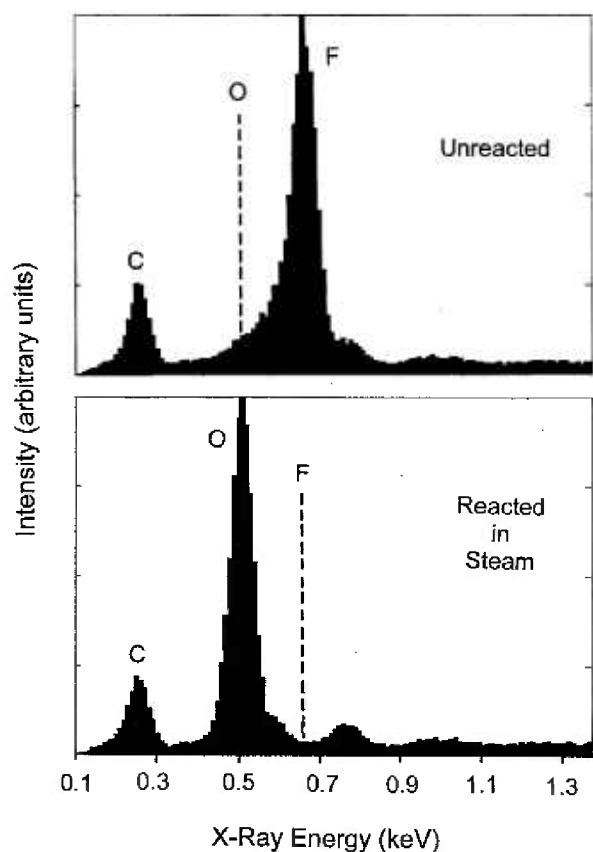

Fig. 10b. Comparative EDS spectra from samples in (a) show that reaction has resulted in essentially complete replacement of F by O at the surface.

to much larger production rates. High-performance films with 1 μm or greater superconductor thickness could find immediate application in second-generation high T_c technology, especially if production costs approach the anticipated $10/kA-m target [24].

11. Summary and Conclusions

Thermodynamic calculations have outlined a stability field for $Ba(OH)_2(liq)$ as a function of p_{H_2O}, p_{HF}, and temperature, based on presently available data. An experiment at 815 °C, p_{H_2O} = 0.1 MPa has provided evidence for the formation of $Ba(OH)_2(liq)$ by defluorination of $BaF_2(s)$, as predicted by the calculations. It is possible that under conditions of high p_{H_2O} and rapid gas flow, the formation of $Ba(OH)_2(liq)$ may occur as an intermediate step in the formation of superconducting $Ba_2YCu_3O_{6.5+x}(s)$ from amorphous (BaF_2, Y, Cu) precursors. The presence of a $Ba(OH)_2$ liquid could be important for $Ba_2YCu_3O_{6.5+x}(s)$ processing for several reasons. It is well known that a liquid phase enhances mobility and can aid in local mass transport and the development of oriented microstructures. The presence of a liquid would be expected to improve the kinetics of $Ba_2YCu_3O_{6.5+x}(s)$ phase formation, although it may be necessary to limit the presence of the liquid phase at some stages during processing to prevent random growth, as opposed to oriented growth. Clearly, it is essential to

control the amount of liquid in order to fully optimize all aspects of $Ba_2YCu_3O_{6.5+x}(s)$ formation using the BaF_2 *ex situ* process. With sufficient data on liquid formation, p_{H_2O} provides an additional parameter, along with precursor F/O composition, gas flow, temperature, time, and p_{O_2}, with which to reproducibly control the processing of $Ba_2YCu_3O_{6.5+x}(s)$.

The calculated phase diagrams require further experimental verification to establish the role of BaF_2 solubility in the liquid, and the precise boundaries of the $Ba(OH)_2$ stability field. Preliminary experiments have indicated that $Ba_2YCu_3O_{6.5+x}(s)$ is stable in the presence of $Ba(OH)_2(liq)$ [25]; it is essential to know the range of conditions under which the $Ba_2YCu_3O_{6.5+x}(s)$ and the $Ba(OH)_2$ stability fields overlap. Based on the extent to which $Ba(OH)_2$-based liquids extend into the phase space of Fig. 2, it may prove possible to design processing routes to control intersection of the PVD and MOD processing paths with the hydroxide liquid phase field. Then the full range of p_{H_2O}-temperature processing space can be explored to determine if there are new processing routes which might lead to further optimization of superconductor formation and film properties.

Acknowledgements

12. References

[1] S. R. Foltyn, E. J. Peterson, J. Y. Coulter, P. N. Arendt, Q. X. Jia, P. C. Dowden, M. P. Maley, X. D. Wu, and D.E. Peterson, Influence of deposition rate on the properties of thick $YBa_2Cu_3O_{7-x}$ films, J. Mater. Res. **12**(11), 2941-2946 (1997).

[2] Y. Iijima, M. Hosaka, N.Tanabe, N. Sadakata, T. Saitoh, O. Kohno, and K. Takeda, Biaxial alignment control of $YBa_2Cu_3O_{7-x}$ films on random Ni-based alloy with textured yttrium stabilized-zirconia films formed by ion-beam-assisted deposition, J. Mater. Res. **12**(11), 2913-2923 (1997).

[3] A. Goyal, D. P. Norton, J. D. Budai, M. Paranthaman, E. D. Specht, D. M. Kroeger, D. E. Christen, Q. He, B. Saffian, F. A. List, D. F. Lee, P. M. Martin, C. E. Klabunde, F. Hartfield, and V. K. Sikka, High critical current density superconducting tapes by epitaxial deposition of $YBa_2Cu_3O_x$ thick films on biaxially textured metals, Appl. Phys. Lett. **69**(12), 1795-1797 (1996).

[4] M. Paranthaman, C. Park, X. Cui, A. Goyal, D. F. Lee, P. M. Martin, T .G. Chirayil, D. T. Verebelyi, D. P. Norton, D. K. Christen, and D. M. Kroeger, $YBa_2Cu_3O_{7-y}$-coated conductors with high engineering current density, J. Mater. Res **15** (12), 2647-2652 (2000).

[5] R. Feenstra, T. B. Lindemer, J. D. Budai, and M. D. Galloway, Effect of oxygen pressure on the synthesis of $YBa_2Cu_3O_{7-x}$

[6] P. C. McIntyre, M. J. Cima, J. A. Smith, R. B. Hallock, M. P. Siegal, and J. M. Phillips, Effect of growth conditions on the properties and morphology of chemically derived epitaxial thin films of $Ba_2YCu_3O_{7-x}$ on (001) $LaAlO_3$, J. Appl. Phys. **71**(4), 1868-1877 (1992).

[7] P. C. McIntyre, M. J. Cima, and A. Roshko, Epitaxial nucleation and growth of chemically derived $Ba_2YCu_3O_{7-x}$ thin films on (001) $SrTiO_3$, J. Appl. Phys. **77** (10), 5263-5272 (1995).

[8] L. Wu, Y. Zhu, V .F. Solovyov, H. J. Wiesmann, A. R. Moodenbaugh, R. L. Sabatini, and M. Suenaga, Nucleation and growth of $YBa_2Cu_3O_x$ on $SrTiO_3$ and CeO_2 by a BaF_2 post-deposition reaction process, J. Mater. Res. **16**(10), 2869-2884 (2001).

[9] L. P. Cook, W. Wong-Ng, and J. Suh, DTA/TGA study of eutectic melting in the system BaF_2-BaO-Y_2O_3-CuO_x-H_2O, in High-Temperature Superconductors—Crystal Chemistry, Processing and Properties, U. Balachandran, H. C. Freyhardt, T. Izumi, and D. C. Labalestier, eds., paper II 4.8 in Materials Research Society Symposium Proceedings **659**, Materials Res. Soc., Warrendale, PA (2001).

[10] W. Wong-Ng, L. P. Cook, J. Suh, I. Levin, M. Vaudin, R. Feenstra, and J. Cline, Phase relationships and phase formation in the system BaF_2-BaO-Y_2O_3-CuO_x-H_2O, in Materials for High-Temperature Superconductor Technologies, M. P. Paranthaman, M. W. Rupich, K. Salama, J. Mannhart, and T. Hasegawa, eds., Materials Research Society Symposium Proceedings **689**, Materials Res. Soc., Warrendale, PA (2002) 337-348.

[11] W. Wong-Ng, L. P. Cook, J. Suh, I. Levin, and R. Feenstra, Melting investigation in the system BaF_2-BaO-Y_2O_3-CuO_x-H_2O, J. Mater. Res. **18**, 1-12 (2005).

[12] D. R. Lide, ed., CRC Handbook of Chemistry and Physics, 84th ed. 2003-2004, CRC Press, Boca Raton, FL (2003) Sec. 4, p. 37.

[13] W. Wong-Ng, I. Levin, M. Vaudin, R. Feenstra, L. P. Cook, and J. P. Cline, High temperature x-ray diffractometer study of phase evolution in $Ba_2YCu_3O_{6.5+x}$ films using the "BaF_2" Conversion Process, Adv. in X-Ray Diffraction **46**, 257-263 (2002).

[14] F. A. List, E. D. Specht, L. Heatherly, K. J. Leonard, S. Sathyamurthy, and D. M. Kroeger, Crystalline phase development during vacuum conversion of thin barium fluoride precursor films on metallic substrates, Physica C **391** (4), 350-362 (2003).

[15] D. Lee and V. Maroni, Reel-to-reel characterization of time-based phase evolution in YBCO coated conductors: the BaF_2 precursor, Superconductivity for Electric Systems 2003 Annual Peer Review, U.S. Dept. Energy, Washington, DC, July 23-25, 2003.

[16] J. J. Ritter, An hermetically sealed inert atmosphere cell for x-ray powder diffraction, Powd. Diff. **3** (1), 30-31 (1988).

[17] Malcom W. Chase, Jr., NIST-JANAF Thermochemical Tables, Fourth Edition, J. Phys. Chem. Ref. Data, Monograph No. 9 (1998).

[18] C. W. Bale, P. Chartrand, S. A. Degterov, G. Eriksson, K. Hack, R. Ben Mahfoud, J. Melancon, A. D. Pelton, and S. Peterson, FactSage thermochemical software and databases, CALPHAD **26**(2), 189-228 (2002).

[19] W. Wong-Ng, I. Levin, R. Feenstra, L. P. Cook, and M. Vaudin, Phase evolution of $Ba_2YCu_3O_{6+x}$ films during the BaF_2 process, Supercond. Sci. Technol. **17**, S548-S556 (2004).

[20] International Centre for Diffraction Data, Newtown Square, PA (2004).

[21] R. S. Roth, C. J. Rawn, F. Beech, J. D. Whitler, and J. O. Anderson, Phase equilibria in the system Ba-Y-Cu-O-CO_2 in air, in Ceramic Superconductors II, M. F. Yan, ed., American Ceramic Society, Wersterville, OH (1988) pp.13-26.

[22] W. Wong-Ng, J. Suh, and L. P. Cook, Subsolidus phase relationships of the BaO-Y_2O_3-CuO_x system under carbonate-free conditions at p_{O_2} = 100 Pa and at p_{O_2} = 21 kPa, Physica C **377**, 107-113 (2002).

[23] S. W. Sofie and F. Dogan, Effect of carbon on the microstructure and superconducting properties of $YBa_2Cu_3O_{7-x}$ melt-textured crystals, Supercond. Sci. Technol. **15**, 735-740 (2002).

[24] A. Sheth and K. Trembath, Economic evaluation of sol-gel based film coating scheme for HTS materials, Supercond. Sci. Technol. **16**, 322-328 (2003).

[25] W. Wong-Ng and L. P. Cook, Phase relations of high T_c superconductors, Superconductivity for Electric Systems 2002 Annual Peer Review, U.S. Dept. Energy, Washington, DC, July 17-19, 2002.

About the authors: *Lawrence Cook and Winnie Wong-Ng are materials scientists in the Ceramics Division of the NIST Materials Science and Engineering Laboratory. Roeland Feenstra is a materials scientist in the Condensed Matter Sciences Division of Oak Ridge National Laboratory. The National Institute of Standards and Technology is an agency of the Technology Administration, U.S. Department of Commerce.*